

The contrasting magnetic fields of superconducting pulsars and magnetars

S. K. Lander^{1*}

¹ *Theoretical Astrophysics, University of Tübingen, Auf der Morgenstelle 10, Tübingen 72076, Germany*

14 January 2021

ABSTRACT

We study equilibrium magnetic field configurations in a neutron star (NS) whose core has type-II superconducting protons. Unlike the equations for normal matter, which feature no special field strength, those for superconductors contain the lower critical field, of order 10^{15} G. We find that the ratio of this critical field to the smooth-averaged stellar field at the crust-core boundary is the key feature dictating the field geometry. Our results suggest that pulsar and magnetar-strength fields have notably different configurations. Field decay for NSs with $B_{\text{pole}} \sim 10^{14}$ G could thus result in substantial internal rearrangements, pushing the toroidal field component out of the core; this may be related to observed magnetar activity. In addition, we calculate the magnetically-induced ellipticities of our models.

Key words:

1 INTRODUCTION

The gradual decrease in the rotation rate of a neutron star is attributed to magnetic dipole radiation and is used to produce an inferred value for the polar-cap field strength. This value is often colloquially referred to as ‘the star’s magnetic field’, whereas it is just an estimate of one component (the dipole) at one location. In the absence of more detailed information, it is this surface dipole value — perhaps with an educated guess about the interior — which is used to try to understand magnetic phenomena in neutron stars: the evolution of their rotation and temperature, the presence or absence of possible magnetic instabilities (Tayler 1973; Wright 1973; Akgün & Wasserman 2008; Akgün et al. 2013), crust-core coupling (Easson 1979) and precession (Mestel & Takhar 1972), to name a few. In magnetars, the most highly magnetised objects known, the magnetic field provides the main reservoir of ‘free’ energy and is likely to play a major role in their observed flaring activity and quasi-periodic oscillations (Thompson & Duncan 1995).

The problem is that we have no guarantee that the inferred polar-cap fields of neutron stars are comparable with their interior fields. Two opposing, but quite feasible scenarios would suggest not. If the star’s magnetic field is mainly confined to the crust the polar-cap value would be larger than the average interior field; by contrast, if the field is mostly buried within the star, for example through ac-

cretion, the polar-cap value would be an underestimate. It has been suggested that understanding these interior fields would help to unify the various observationally disparate classes of NS (Kaspi 2010; Viganò et al. 2013).

To date we have clues about a neutron star’s interior field, but no observations that provide an unambiguous probe of it. Instead, we must resort to finding candidate configurations through modelling. One approach would be an evolutionary one, trying to follow the star from its birth in a supernova, through any early convective or dynamo phases (Spruit 2009) and the later secular evolution of the system (Pons, Miralles & Geppert 2009). In this work we attack the problem from a different angle, seeking solutions to a model neutron star in dynamical equilibrium. To be astrophysically relevant solutions, these equilibria would also have to be stable, although we do not study that here.

Specifically, we aim to account for proton superconductivity in a NS’s core, and the effect this has on magnetic-field equilibria. As discussed in the next section, it has been believed for decades that NSs contain a large superfluid-superconducting inner region, and magnetic fields are known to behave very differently in superconducting and normal matter. Despite this, most studies of NS equilibria are rooted in the classical physics of normal conductors. Following a brief discussion on superconductivity we describe accounting for this in our NS model, which consists of two effectively decoupled fluids: protons and neutrons each obey their own polytropic relation and magnetic forces act only on the protons; if we included entrainment there would be an effective force on the neutrons too. We focus on our treatment of the

* samuel.lander@uni-tuebingen.de

crust-core boundary, which is designed to minimise any current sheet appearing in this region. Our new boundary treatment provides the main difference in approach between this work and the preceding paper (Lander 2013), where we had implicitly assumed magnetar-strength stellar fields, around $\sim 10^{15}$ G at the crust-core boundary. After discussing our method of solution we present results for poloidal and mixed poloidal-toroidal field configurations, comparing weak and strong field configurations in a superconductor with corresponding normal-matter models. We conclude by discussing the possible implications of this work for magnetar activity.

2 SUPERCONDUCTIVITY IN NEUTRON STARS

There are a number of compelling reasons to believe that the interior of a neutron star contains a neutron superfluid and a superconducting proton fluid. From the theoretical side, the broad picture we have of the core region remains the one outlined by the seminal work of Baym, Pethick & Pines (1969), but the first predictions of superfluidity in neutron stars (Migdal 1959; Ginzburg & Kirzhnits 1965) actually predated the discovery of pulsars. Although NSs are certainly hot by terrestrial standards, around 10^8 K, this is in fact extremely cold for such dense objects; their Fermi temperature is about 10^{12} K. NS matter is therefore highly degenerate, and the microscopic theory for terrestrial superconductivity (Bardeen, Cooper & Schrieffer 1957) implies that both neutrons and protons will form Cooper pairs, leading to a neutron superfluid and proton superconductor.

Before discussing the details of superconductivity in neutron stars, we first outline a few key results in the theory of terrestrial low-temperature superconductivity (two good introductory texts on the topic are Tinkham (1996) and Tilley & Tilley (1990)). There are two important length-scales in a superconductor: the penetration depth λ , the characteristic lengthscale over which the Meissner effect causes exponential drop-off of the field strength as one moves into the superconducting region; and the coherence length ξ , the characteristic lengthscale for variation of the superconducting-particle wavefunction, or the ‘radius of the Cooper pair’. The ratio of these two lengthscales forms the Ginzburg-Landau parameter

$$\kappa_{GL} = \frac{\lambda}{\xi} \quad (1)$$

and dictates the type of superconductivity. If $\kappa_{GL} < 1/\sqrt{2}$ type-I superconductivity prevails: the surface energy of the superconductor is positive and large regions are devoid of magnetic flux. If instead $\kappa_{GL} > 1/\sqrt{2}$ we have a type-II superconductor: the surface energy is negative and the superconductor is unstable to the increase of its surface area through the formation of fluxtubes, provided that the magnetic field strength $B > H_{c1}$, the ‘lower critical field’. The magnetic field is thus able to penetrate the bulk of the superconductor through these fluxtubes. As the field strength is increased the fluxtubes become more densely packed, until finally at $B = H_{c2}$ (the ‘upper critical field’) superconductivity is destroyed.

Returning to astrophysics, the longest-standing piece of evidence in favour of superfluidity in neutron star cores

is pulsar glitches — rapid events in which the star is seen to spin up slightly (in contrast to its long-term decrease in rotation rate). This is widely thought to represent a transfer of angular momentum from a more rapidly-spinning internal superfluid component to the crust (Anderson & Itoh 1975). More recently, the rapid cooling of the Cassiopeia A neutron star has been attributed to the onset of neutron superfluidity, together with protons already in a superconducting state (Page et al. 2011; Shternin et al. 2011). Even at magnetar field strengths, neutron stars are believed to become cold enough to admit superfluid-superconducting regions within a few hundred years of their birth (Ho, Glampedakis & Andersson 2012).

The protons of a NS’s outer core are expected to form a type-II superconductor, with values for the two critical fields being roughly $H_{c1} \sim 10^{15}$ G and $H_{c2} \sim 10^{16}$ G, but the timescale for Meissner expulsion is so long that the fluxtube state is still expected to be metastable when $B < H_{c1}$ (Baym, Pethick & Pines 1969; Jones 1987). Because of its regularity, one can take an average over this fluxtube array to determine the macroscopic magnetic force acting on a type-II superconductor (Easson & Pethick 1977; Mendell 1991; Akgün & Wasserman 2008; Glampedakis, Andersson & Samuelsson 2011):

$$\mathfrak{F}_{\text{mag}} = -\frac{1}{4\pi} \left[\mathbf{B} \times (\nabla \times \mathbf{H}_{c1}) + \rho_p \nabla \left(B \frac{\partial H_{c1}}{\partial \rho_p} \right) \right], \quad (2)$$

where \mathbf{B} represents the smooth-averaged magnetic field and $\mathbf{H}_{c1} = H_{c1} \hat{\mathbf{B}}$ ($\hat{\mathbf{B}} = \mathbf{B}/B$, the magnetic field unit vector). This force is clearly not simply a rescaling of the normal-matter Lorentz force. There is also likely to be an inner core region with type-I superconducting protons, with alternating $B = 0$ and $B \neq 0$ domains, but without the regular structure of a fluxtube array (Sedrakian 2005). As yet there is no equivalent averaged magnetic force for this case.

3 NEUTRON STAR MODEL

3.1 Assumptions

We model a neutron star as a self-gravitating, stationary and axisymmetric fluid body, with parallel rotation and magnetic symmetry axes. We will adopt cylindrical polar coordinates (ϖ, ϕ, z) , aligning the star’s symmetry axis with the coordinate z -axis. The star is non-relativistic and has zero electrical resistivity. It has a core composed of type-II superconducting protons, superfluid neutrons and normal electrons; this is effectively a two-fluid system, since the inertia of the electrons is negligible and their chemical potential can be absorbed into that of the protons. Beyond a certain density in a neutron star, this admixture of particles may give way to an inner core with exotic particles or a region with type-I superconductivity. We ignore any such physics for simplicity, but it is possible that such high densities may not be attained in large regions of the star anyway; the recently observed two-solar-mass pulsars suggests neutron stars obey a fairly stiff equation of state with relatively low central density (Demorest et al. 2010; Antoniadis et al. 2013).

The core is surrounded by an elastic crust of normal matter, which we assume to be relaxed. Note that a stressed

crust evolves secularly in a manner governed by Hall drift and Ohmic decay — with the former term expected to be dominant, the crustal field would eventually settle into a ‘Hall equilibrium’ configuration (Gourgouliatos et al. 2013). Since we assume there are no elastic stresses, the equations for the crust reduce to those of a single fluid. We can, therefore, model the entire star as a two-fluid equilibrium:

1. the superfluid neutrons extend from the centre of the star to the crust-core boundary;
2. the ‘proton’ fluid represents the proton-and-electron fluid in the core, where it is subject to the fluxtube tension force;
3. beyond the crust-core boundary, the same ‘proton’ fluid is reassigned to become the single-fluid crust, representing an unstrained ion lattice and obeying the Lorentz force of normally-conducting matter.

Our two-fluid model gives us the freedom to choose different pressure-density relations for the neutrons and protons, making us better able to mimic a ‘realistic’ NS profile than with a polytropic equation of state (Lander, Andersson & Glampedakis 2012). It also enables us to introduce composition-gradient stratification in the stellar core. For very young neutron stars it would be more appropriate to allow for stratification from temperature/entropy gradients (Reisenegger 2009; Mastrano et al. 2011; Yoshida, Kiuchi & Shibata 2012); in this case the star would also be too hot to form the multifluid state studied here. Our work is applicable to neutron stars over a few hundred years old, including magnetars (Ho, Glampedakis & Andersson 2012).

3.2 General equations

As described above, our neutron star model is a two-fluid system in equilibrium. This is therefore governed by a pair of Euler equations — one for the neutrons (denoted with a subscript n) and another for the ‘proton’ fluid (subscript p), used to describe the combined proton-electron fluid in the core and the relaxed ion lattice in the crust:

$$\nabla \left(\tilde{\mu}_n + \Phi - \frac{\varpi^2 \Omega_n^2}{2} \right) = 0, \quad (3)$$

$$\nabla \left(\tilde{\mu}_p + \Phi - \frac{\varpi^2 \Omega_p^2}{2} \right) = \frac{\mathfrak{F}_{\text{mag}}}{\rho_p}, \quad (4)$$

where $\tilde{\mu}_x$ is the chemical potential of each particle species ($x \in \{n, p\}$), Φ gravitational potential, Ω_x each fluid’s rotation rate and $\mathfrak{F}_{\text{mag}}$ the magnetic force; the form of this force will be the only difference between the normal and superconducting cases. We are also implicitly assuming there is no entrainment, a coupling between particle species which would lead to a magnetic force on the neutrons for a superfluid-superconducting core (Glampedakis, Andersson & Samuelsson 2011). We will only consider the case of corotating fluids, i.e. $\Omega_n = \Omega_p \equiv \Omega$.

Even in the absence of any other coupling mechanisms, the two fluids are indirectly linked through Poisson’s equation, as they both feel the same gravitational potential:

$$\nabla^2 \Phi = 4\pi G \rho = 4\pi G (\rho_n + \rho_p). \quad (5)$$

Instead of using the two individual Euler equations, we will work with the neutron-fluid Euler and a ‘difference-Euler’,

given by (4) minus (3):

$$\nabla (\tilde{\mu}_p - \tilde{\mu}_n) = \frac{\mathfrak{F}_{\text{mag}}}{\rho_p}. \quad (6)$$

Taking the curl of this equation shows that $\mathfrak{F}_{\text{mag}}/\rho_p$ is irrotational and so (as in the single-fluid case) there exists a scalar M such that

$$\frac{\mathfrak{F}_{\text{mag}}}{\rho_p} = \nabla M. \quad (7)$$

The magnetic force — whether the normal-matter Lorentz force or the superconducting fluxtube tension — therefore depends on a scalar function M and the proton-fluid density ρ_p , as opposed to the single-fluid case where the dependence is on the total mass density: $\mathfrak{F}_{\text{mag}}/\rho = \nabla M$. The single-fluid versions of the magnetic equations we present here may be found simply by replacing any ρ_p terms with the total ρ .

Another universal result is the Maxwell equation

$$\nabla \cdot \mathbf{B} = 0. \quad (8)$$

Since our system is axisymmetric we may use this equation to write \mathbf{B} in terms of a streamfunction u :

$$\mathbf{B} = \frac{1}{\varpi} \nabla u \times \mathbf{e}_\phi + B_\phi \mathbf{e}_\phi. \quad (9)$$

This implies that whatever the magnetic force, we have $\mathbf{B} \cdot \nabla u = 0$; field lines are parallel to contours of the streamfunction.

We close our system with an equation of state. As in previous papers (Lander, Andersson & Glampedakis 2012; Lander 2013), we choose a two-fluid generalisation of a polytrope. Specifically, we choose an energy functional

$$\mathcal{E} = \mathcal{E}(\rho_n, \rho_p, w_{np}^2) = k_n \rho_n^{1+1/N_n} + k_p \rho_p^{1+1/N_p}. \quad (10)$$

In general the functional would involve a term in the relative velocity between the particle species $\mathbf{w}_{np} \equiv \mathbf{v}_n - \mathbf{v}_p$, coupling the two fluids (like entrainment); in our simple choice for \mathcal{E} this term is zero. The chemical potentials of the species are now defined through \mathcal{E} :

$$\tilde{\mu}_x \equiv \left. \frac{\partial \mathcal{E}}{\partial \rho_x} \right|_{\rho_y}, \quad (11)$$

where x represents one particle species and y the other.

For our equation of state, then, each particle species obeys its own barotropic relation: $\tilde{\mu}_n = \tilde{\mu}_n(\rho_n)$ and $\tilde{\mu}_p = \tilde{\mu}_p(\rho_p)$. Our chosen energy functional may therefore be thought of as a ‘double polytrope’ in the two fluids (Prix, Comer & Andersson 2002). Note that the total pressure is not generally a function of the total density though, $P \neq P(\rho)$. Our equation of state enables us to derive results for a stratified two-fluid star which are equivalent to those for a single-fluid barotropic star, although one should be aware that the introduction of proton-neutron coupling could lead to qualitative changes in the resulting equilibria.

3.3 Normal crust

As described earlier, we are treating the neutron star crust as being relaxed, so that its equilibrium state involves only fluid and magnetic forces, with no shear stresses. Unlike the core

protons, the crust is expected to be composed of normally-conducting matter, which we treat as a single fluid. In this familiar case $\mathfrak{F}_{\text{mag}}$ is the Lorentz force, given by

$$\mathfrak{F}_{\text{mag}} = \frac{1}{4\pi}(\nabla \times \mathbf{B}) \times \mathbf{B}. \quad (12)$$

For axisymmetric equilibria, the behaviour of the magnetic field may be encapsulated in a single differential equation, the *Grad-Shafranov equation* (Grad & Ruben 1958; Shafranov 1958):

$$\Delta_* u = -4\pi\rho_p\varpi^2 \frac{dM}{du} - f_N \frac{df_N}{du}, \quad (13)$$

where f_N is related to the toroidal-field component through

$$f_N(u) = \varpi B_\phi, \quad (14)$$

and Δ_* is a differential operator:

$$\Delta_* \equiv \frac{\partial^2}{\partial \varpi^2} - \frac{1}{\varpi} \frac{\partial}{\partial \varpi} + \frac{\partial^2}{\partial z^2} \quad (15)$$

— this is the Laplacian operator with the sign of the second term reversed. For later comparison, we note from equations (9) and (14) that the magnitude of the magnetic field is given by

$$B = \frac{\sqrt{|\nabla u|^2 + f_N^2(u)}}{\varpi}. \quad (16)$$

The Grad-Shafranov equation describes mixed poloidal-toroidal fields, or purely poloidal fields by taking $f_N(u) = 0$. In the special case of a purely toroidal field there is no separate equation, and the Lorentz force term in the Euler equation reduces to the form:

$$M = -\frac{1}{4\pi} \int_0^{\rho_p \varpi^2} \frac{\eta_N(\beta)}{\beta} \frac{d\eta_N}{d\beta} d\beta, \quad (17)$$

for some free function $\eta_N = \eta_N(\rho_p \varpi^2)$. This function is related to the magnetic field strength through

$$B_\phi = \frac{\eta_N(\rho_p \varpi^2)}{\varpi}. \quad (18)$$

A detailed derivation of these relations is given in Lander & Jones (2009).

3.4 Type-II superconducting core

We assume that the protons throughout the core form a type-II superconductor, with the magnetic field quantised into fluxtubes, resulting in the magnetic force (2) discussed in section 2. Although this force is more complicated than the Lorentz force, we may use many of the same tricks as for the Grad-Shafranov equation. Again, the problem splits into two cases: one for purely toroidal fields and another for poloidal/mixed fields. We relegate the full derivations to appendix A and report just the key results here.

3.4.1 Toroidal fields

The case of purely toroidal fields in a superconductor is very similar to that for normal matter. There is no separate equation for the magnetic field; the proton Euler equation simply

gains one extra term related to the magnetic force (recall that $\nabla M = \mathfrak{F}_{\text{mag}}/\rho_p$):

$$M = -\frac{h_c}{4\pi} \int_0^{\rho_p \varpi} \frac{1}{\beta} \frac{d\eta}{d\beta} d\beta \quad (19)$$

for some free function $\eta = \eta(\rho_p \varpi)$. The corresponding magnetic field strength is

$$B_\phi = \frac{\eta(\rho_p \varpi)}{\rho_p \varpi}. \quad (20)$$

Configurations with this type of magnetic field were studied in earlier work (Akgün & Wasserman 2008; Lander, Andersson & Glampedakis 2012) and are not the subject of the present study; we include the relations for the sake of completeness.

3.4.2 Mixed poloidal-toroidal fields

The derivation of an equation governing mixed poloidal-toroidal fields in a superconductor is similar, in many ways, to that for the normal-matter Grad-Shafranov equation. One key difference is that the magnetic-force function M (see equation (7)) is no longer a function of the streamfunction u . Since our desired end result is an equation in terms of u and functions thereof, we instead define a related quantity which involves M but is also a function of u :

$$y(u) = \frac{4\pi M}{h_c} + B. \quad (21)$$

The local field strength B appears many times, in combination with the proton density, so for brevity we define the quantity

$$\Pi \equiv \frac{B}{\rho_p}. \quad (22)$$

Using these quantities, we show in appendix A that a mixed poloidal-toroidal field is governed by the following equation:

$$\Delta_* u - \frac{\nabla \Pi \cdot \nabla u}{\Pi} = -\varpi^2 \rho_p \Pi \frac{dy}{du} - \Pi^2 f \frac{df}{du}. \quad (23)$$

The free function $f(u)$ is again related to the toroidal field component, but differs from the normal-matter result by a factor of Π :

$$f(u) = \frac{\varpi B_\phi}{\Pi}. \quad (24)$$

Equation (23) is the equivalent of the Grad-Shafranov equation when the stellar matter (protons in our two-fluid system) is a type-II superconductor. The most significant difference from the normal case is the presence of terms related to the field strength B (in the quantity Π). Using equations (9) and (24), we see that B is indirectly related to u :

$$B = \frac{|\nabla u|}{\sqrt{\varpi^2 - f^2(u)/\rho_p}}, \quad (25)$$

which may be compared with the normal-matter result (16). The presence of B therefore represents an additional degree of nonlinearity in the equation; in attempting to solve (23), we may anticipate particular difficulties associated with the $\nabla \Pi \cdot \nabla u / \Pi$ term. Another difference is that whereas the magnetic force appears explicitly in the Grad-Shafranov equation, through the function M , it does not in the corresponding equation for superconducting matter.

The results reported in this section agree with expressions in Henriksson & Wasserman (2013), who specialised to poloidal fields and used a different method of solution, which did not require the explicit form of equation (23) in terms of the streamfunction.

3.5 Crust-core boundary conditions

We need to solve for the magnetic field in three distinct domains: the superconducting core, normal crust and vacuum outside the star. In a spherical model we would be able to put the surface and crust-core boundaries at some specified radius, but since we wish to allow for deformations of the star we define these boundaries in terms of proton density contours instead. Denoting the equatorial surface by r_{eq} , the stellar surface and crust-core boundary are given by the pairs of (ϖ, z) coordinates satisfying

$$\rho_{\text{p}}^{\text{surface}}(\varpi, z) = \rho_{\text{p}}(r_{\text{eq}}, 0) = 0, \quad (26)$$

$$\rho_{\text{p}}^{\text{cc}}(\varpi, z) = \rho_{\text{p}}(0.9r_{\text{eq}}, 0). \quad (27)$$

The magnetic equation to be solved is then:

$$\Delta_* u = \begin{cases} -\varpi^2 \rho_{\text{p}} \Pi y'(u) - \Pi^2 f(u) f'(u) + \frac{\nabla \Pi \cdot \nabla u}{\Pi} & \text{core} \\ -4\pi \varpi^2 \rho_{\text{p}} M'_N(u) - f_N(u) f'_N(u) & \text{crust} \\ 0 & \text{exterior} \end{cases} \quad (28)$$

At the crust-core boundary of a neutron star there is likely to be complicated microphysics, with forces pinning fluxtubes to the crust and perhaps a current sheet. Since we do not yet have a good model for these effects, we consider it safer first to omit these and model the simplest crust-core boundary: requiring force balance, and for the field to remain divergence-free (equivalent to imposing continuity of the field component perpendicular to the boundary). The latter condition is satisfied automatically by working with the streamfunction. A more detailed discussion of the crust-core boundary, including aspects of the microphysics of the region, is given in Henriksson & Wasserman (2013).

3.5.1 Earlier treatment of boundary

In Lander (2013), force balance was ensured by arguing that whilst \mathbf{B} and \mathbf{H} are distinct quantities in the superconducting core, they should be equal in the crust. In the core

$$\mathbf{H}_{c1} = \frac{H_{c1}}{B} \mathbf{B}; \quad (29)$$

this can be matching smoothly to the crust by requiring that $\mathbf{H}_{c1} \rightarrow \mathbf{H}^{\text{crust}} = \mathbf{B}^{\text{crust}}$ at the boundary, i.e. $H_{c1} \rightarrow B$. This was done by making appropriate choices of the core functions $y(u), f(u)$ in terms of the crust functions $M_N(u), f_N(u)$. This only allows for smooth matching without an associated surface current provided that $B^{\text{cc}} \sim 10^{15}$ G, however; potentially appropriate only for magnetars. Assuming $H_{c1} \rightarrow B$ at the crust-core boundary effectively prevented us from finding solutions with a sharp transition, like those of Henriksson & Wasserman (2013).

3.5.2 New treatment of boundary

In this paper we use a more general treatment than that of Lander (2013), allowing us to study the more typical case where $B < H_{c1}$ at the boundary. Previous work on poloidal fields in superconducting stars specialised to this case, using geometric techniques to solve along individual field lines and formulating the boundary conditions accordingly: Roberts (1981) argued that to match a superconducting region to vacuum, all field lines should cross the surface perpendicularly, whilst Henriksson & Wasserman (2013) discuss a class of solutions where field lines hit the boundary of the superconducting domain vertically. Our approach is different and does not allow us to specify the geometry of field lines *a priori*.

At the boundary we want the magnetic force in the core and the Lorentz force in the crust to balance. Using square brackets and a superscript ‘cc’ to denote evaluation at the crust-core boundary, we have:

$$[\rho_{\text{p}}^{\text{core}} \nabla M_{sc}]^{\text{cc}} = [\rho_{\text{p}}^{\text{crust}} \nabla M_N(u)]^{\text{cc}}. \quad (30)$$

At this stage we allow for a possible jump in the density at the crust-core boundary (expected from more realistic equations of state, e.g. Akmal, Pandharipande & Ravenhall (1998)), though in our models ρ_{p} is smooth everywhere. Using the definition of $y(u)$, we may rewrite this as

$$[\nabla B^{\text{core}}]^{\text{cc}} = \left[\left(\frac{dy}{du} - \frac{4\pi \rho_{\text{p}}^{\text{crust}}}{h_c \rho_{\text{p}}^{\text{core}}} \frac{dM_N}{du} \right) \nabla u \right]^{\text{cc}}. \quad (31)$$

Dotting \mathbf{B} into both sides, we see that B^{core} at the crust-core boundary should be a function of the streamfunction u , since $[\mathbf{B} \cdot \nabla B^{\text{core}}]^{\text{cc}} = \mathbf{B} \cdot \nabla u = 0$. This is not straightforward to enforce, because the crust-core boundary is given by a contour of ρ_{p} , not of u . We will look for a polynomial approximation $\tilde{B}^{\text{cc}}(u)$ to the actual value of B along the core side of the boundary, as evaluated using relation (25), which we term B^{cc} . Let us assume a quadratic relation between $\tilde{B}^{\text{cc}}(u)$ and u :

$$\tilde{B}^{\text{cc}}(u) = c_0 + c_1 u + c_2 u(u - u_{\text{eq}}^{\text{cc}}), \quad (32)$$

where c_0, c_1, c_2 are constants and $u_{\text{eq}}^{\text{cc}}$ is the value of u at the equatorial crust-core boundary. Now, the streamfunction u attains its maximum in the centre of the closed-field line region and is always zero along the pole — at this latter location we have $\tilde{B}^{\text{cc}}(u) = c_0$ and so we choose

$$c_0 = B_{\text{pole}}^{\text{cc}}. \quad (33)$$

We now ensure agreement between $\tilde{B}^{\text{cc}}(u)$ and B^{cc} at the equator by choosing

$$c_1 = \frac{B_{\text{eq}}^{\text{cc}} - c_0}{u_{\text{eq}}^{\text{cc}}}. \quad (34)$$

Finally, within our quadratic approximation we can also ensure that $\tilde{B}^{\text{cc}}(u)$ and B^{cc} coincide at some middle point (e.g. at $\theta = \pi/4$) by fixing c_2 :

$$c_2 = \frac{B_{\text{mid}}^{\text{cc}} - c_0 - c_1 u_{\text{mid}}^{\text{cc}}}{u_{\text{mid}}^{\text{cc}}(u_{\text{mid}}^{\text{cc}} - u_{\text{eq}}^{\text{cc}})}. \quad (35)$$

Over successive steps within our iterative scheme (see section B for details) we have found this expression for $\tilde{B}^{\text{cc}}(u)$ provides a moderately good approximation to B along the crust-core boundary, with a discrepancy typically less than 10%; see figure 1. Any discrepancy would result in an undesired, unmodelled current sheet at the boundary, so

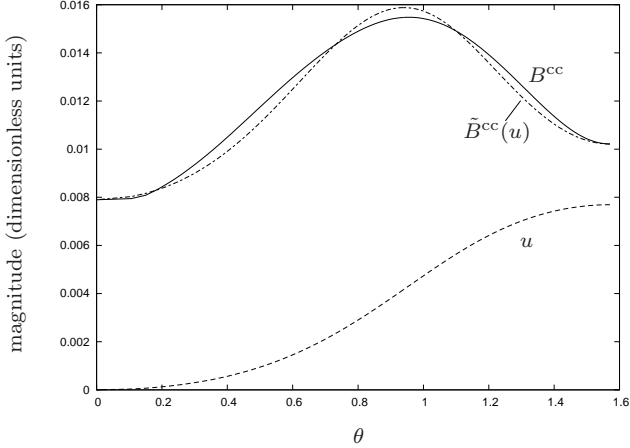


Figure 1. Quantities along the crust-core boundary, from the pole ($\theta = 0$) to the equator ($\theta = \pi/2$). To impose force balance across the boundary we need to find a function $\tilde{B}^{cc}(u)$ of the streamfunction u which approximates the actual value B^{cc} of the magnetic field there; see section 3.5.2.

we wish to minimise this. We are now able to ensure force balance at the crust-core boundary by choosing

$$y(u) = \tilde{B}^{cc}(u) + \frac{4\pi}{h_c} \left[\frac{\rho_p^{core}}{\rho_p^{crust}} \right]^{cc} M_N(u). \quad (36)$$

Next, for a mixed poloidal-toroidal field the crust-core discontinuity in B_ϕ is given by:

$$[B_\phi^{core} - B_\phi^{crust}]^{cc} = \left[\frac{1}{\varpi} \left(\frac{B^{core}}{\rho_p^{core}} f_{sc}(u) - f_N(u) \right) \right]^{cc}. \quad (37)$$

and so we can ensure continuity of the toroidal component by choosing

$$f(u) = [\rho_p^{core}]^{cc} \frac{f_N(u)}{B^{cc}(u)}. \quad (38)$$

Our original system of equations (28) contained four free functions of the streamfunction. To avoid any current sheets at the boundary, however, equations (36) and (38) tell us that only two of these may be chosen independently. We will choose the functional forms in the crust $M_N(u)$, $f_N(u)$ and use these to fix the core functions $y(u)$, $f(u)$; mathematically, it would be equivalent to choose the core functions and fix those in the crust, but this proved to be less numerically stable.

3.6 Numerics

We cast the magnetic-field equation (28) and the other equilibrium equations (3), (5) and (6) into integral form and solve them using a non-linear iterative scheme. The foundation of our code is the self-consistent field method (Hachisu 1986), but extended considerably to solve for superfluid-superconducting stars with magnetic fields. Since our method is not perturbative, we can consistently allow for the back-reaction of the field on the fluid. We are also able to include the contributions from higher multipoles with no additional difficulty; we typically perform a sum up to an angular index $l = 16$. A more detailed description is given in appendix B.

Within the code we use dimensionless variables, non-dimensionalising all quantities by using an appropriate combination of powers of the gravitational constant, the equatorial surface radius and the total central density. For all results with physical units, we have redimensionalised to a 1.4-solar-mass NS with a radius of 10 km; more details are given in Lander, Andersson & Glampedakis (2012).

4 RESULTS

4.1 Choices for the free functions

Within our model of a superconducting neutron star, the magnetic field is specified by the single equation (28). As discussed above, crust-core boundary conditions mean that just two of the four functions of the streamfunction may be chosen independently, with the other two related to these. These free functions are $M_N(u)$, dictating the strength and distribution of the magnetic force throughout the star (indirectly related to the poloidal field component), and $f_N(u)$, dictating the strength of the toroidal-field component.

Some freedom is possible in choosing these, although their effect on the final equilibrium is not dramatic. Since equation (28) involves the derivative $M'_N(u)$, we need $M_N(u)$ to be a power of u greater than or equal to unity; indeed, we will usually take $M_N(u) = \kappa u$, where κ is a constant which will set the magnitude of the magnetic force (and hence the field strength). The simplest choice for the other function is $f_N(u) = 0$, which leads to a purely poloidal field. For mixed-field configurations, we need to ensure $f_N(u)$ is zero outside the star, to avoid an exterior toroidal field and corresponding electric current¹. This is done by fitting $f_N(u)$ to u_{int} , the largest u -contour (i.e. field line) which closes within the star:

$$f_N(u) = \begin{cases} a(u - u_{\text{int}})^{\zeta+1} & \text{for } u \geq u_{\text{int}} \\ 0 & \text{for } u < u_{\text{int}}. \end{cases} \quad (39)$$

Note that the exponent must, again, be greater than unity, since our equations also involve $f'_N(u)$. ζ fixes the steepness of the toroidal-field profile and is set to 0.1 in this work; a dictates the strength of the toroidal component.

4.2 Purely poloidal fields

We begin this section with a reminder of a typical poloidal-field configuration in a *normally-conducting* two-fluid star, in order to be able to make a direct comparison with our new results for a superconducting model. In figure 2 we show the magnitude and direction of an equilibrium poloidal field in a model NS subject to the normal-matter Lorentz force in both core and crust, with $M_N(u) = \kappa u$. The region of field lines that close within the star is centred at a dimensionless equatorial radius $r \approx 0.75$ and the transition between core and crust is smooth. The field geometry is essentially independent of the field strength.

¹ Real neutron stars *do* have an exterior current distribution, the magnetosphere, and $f_N(u)$ could be chosen to account for this (Glampedakis, Lander & Andersson 2013). Here we focus for simplicity on the interior equilibrium and assume a vacuum exterior.

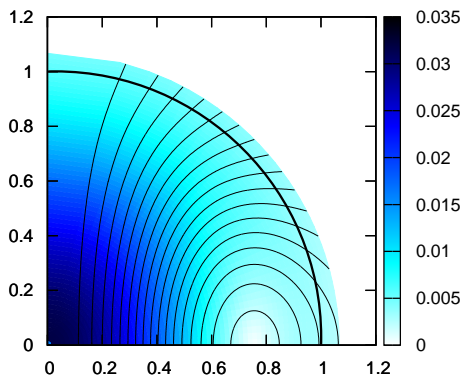


Figure 2. A poloidal magnetic field in a neutron star with a two-fluid core and single-fluid crust, but obeying normal MHD in both domains. As for all other poloidal-field models, we show the field magnitude with the colour scale and its direction with the field lines. The stellar surface is shown with the arc at dimensionless radius $r = 1.0$. The crust-core boundary is at $r = 0.9$, but to avoid cluttering the figure it is not plotted. The field strength volume-averaged over the star, \bar{B} , is 10^{16} G here, but the corresponding plots for $\bar{B} = 10^{14}$ G and 10^{17} G are indistinguishable.

Note that although all our models involve a two-fluid core, the neutrons play a virtually negligible role in the field configurations presented in this paper, because their influence on the protons is only indirect, through Poisson’s equation (5). The inclusion of entrainment would provide a more direct coupling between the two fluids, and we anticipate the distribution of the neutrons would then have some direct effect on the magnetic field.

Using the same functional form $M_N(u) = \kappa u$, we now consider a star whose core protons form a type-II superconductor and hence are subject to a fluxtube tension force instead of the Lorentz force; the results are plotted in figure 3. The three models only differ in their field strength — in particular, the important criterion is the relative magnitude of the smooth-averaged field B to the critical field H_{c1} at the crust-core boundary. H_{c1} is density-dependent and therefore constant along the boundary, but B is not; for this reason we use the average value $\langle B^{cc} \rangle$ for comparisons.

In the left-hand plot of figure 3 we show a star where $\langle B^{cc} \rangle / H_{c1}^{cc} > 1$; in this case the ratio is 5.7. The field direction and magnitude are both smooth across the boundary and the closed-field line region penetrates the core; the configuration is qualitatively similar to the normal-matter model shown in figure 2. It also resembles the poloidal-field solution presented in Lander (2013), where a strong magnetic field had been assumed (see section 3.5.1).

The middle plot shows a star with $\langle B^{cc} \rangle / H_{c1}^{cc} \sim 1$ (specifically, 0.7 in this case). The field lines kink slightly across the crust-core boundary and the closed field lines are pushed outwards. Finally, the right-hand plot is for a star with $\langle B^{cc} \rangle / H_{c1}^{cc} < 1$ (the ratio is 0.4 in this particular model), probably the typical case for pulsars. The closed-field line region has been completely pushed out into the normally conducting crust, whilst no field lines close in the core. The field strength is highest in the vicinity of the crust-core boundary.

The left-hand plot of figure 3, like figure 2, shows field lines hitting the crust-core boundary perpendicularly in the region of the pole and tangentially at the equator. By contrast, in the right-hand plot of figure 3 all field lines hit the boundary approximately perpendicularly, consistent with the expectation of Roberts (1981). Furthermore, with no field lines closing in the core, this field configuration is encouragingly similar to both those presented in Henriksson & Wasserman (2013) and Roberts (1981).

Figure 3 suggests that the interior field structure of a superconducting star can change dramatically as the field strength is lowered, with the closed-field line region being ‘expelled’ from the core into the crust. Note that this is *not* the Meissner effect! To check that this result is not a peculiarity of the functional choice $M_N(u) = \kappa u$, we plot a sequence of equilibria for $M_N(u) = \kappa u^2$ in figure 4. From left to right we show ‘high’ ($\langle B^{cc} \rangle > H_{c1}^{cc}$), ‘medium’ ($\langle B^{cc} \rangle \sim H_{c1}^{cc}$) and ‘low’ ($\langle B^{cc} \rangle < H_{c1}^{cc}$) field strengths, as in figure 3. Although the interior field distribution is different, the general trend for the closed field lines to be pushed out into the crust remains.

The sequences of equilibria shown so far are non-rotating and unstratified, with $N_n = N_p = 1$. For the last two equilibrium models in this section, we study the effect of relaxing these restrictions, both in the low-field case $\langle B^{cc} \rangle < H_{c1}^{cc}$. Firstly we consider a star with composition-gradient stratification in the core, matched to a single-fluid unstratified crust as always. We take $N_n = 0.6$ and $N_p = 1.5$, since an earlier study (Lander, Andersson & Glampedakis 2012) found that models with $N_n < N_p$ mimic realistic equations of state more closely than those with $N_n \geq N_p$. The resultant field configuration — figure 5 — is rather similar to that of the unstratified star shown in the right-hand panel of figure 3.

Our last poloidal-field equilibrium is for a rapidly-rotating unstratified star, with both neutron and proton fluids corotating rigidly. Rotation in a superconductor induces a new contribution to the magnetic field known as the London field — but since this is predicted to be around 1 G or less (Sauls 1989; Glampedakis, Andersson & Samuelsson 2011) it is completely negligible for our purposes. Our rotating model, whose field configuration is shown in figure 6, is noticeably oblate, with the ratio of the polar to equatorial surface radii $r_{\text{pole}}/r_{\text{eq}} = 0.85$. For our canonical NS parameters this corresponds to a rotation rate of 1000 Hz. The stellar rotation also distorts the crust-core boundary away from a spherical shape, and this is the main difference in appearance between this model and the right-hand side model of figure 3. The closed field lines remain confined to the crust.

Finally, we calculate the magnetically-induced distortion within our models. This serves two purposes: the qualitative scaling provides a sanity check of our results and the quantitative results give us an indication of the possible strength of gravitational radiation from a magnetically-distorted neutron star (Bonazzola &ourgoulhon 1996). First we recall the definition of the mass quadrupole moment tensor:

$$Q_{jk} = \int \rho x_j x_k \, dV \quad (40)$$

where x_j, x_k are Cartesian coordinates. As a measure of

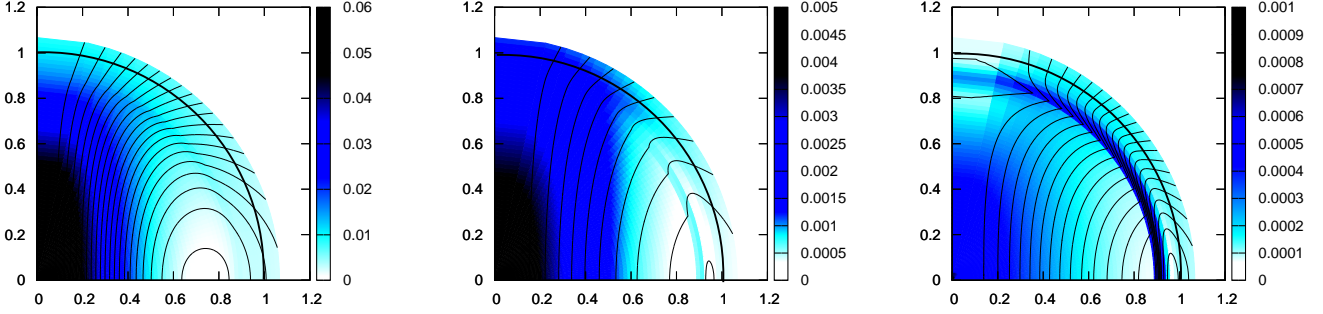


Figure 3. Poloidal magnetic fields in a star with a superconducting core and normal crust, with the boundary between the two located at a dimensionless radius $r = 0.9$ and the surface at $r = 1.0$. We choose $M_N(u) = \kappa u$. Unlike the normal-matter case in figure 2, the equilibria here are qualitatively different for different field strengths, depending on the average ratio of B to H_{c1} at the crust-core boundary. The value of this quantity $\langle B^{cc} \rangle / H_{c1}^{cc} = 5.7, 0.7, 0.4$ for the left, middle and right panels, respectively. As this ratio is decreased the field lines become sharper across the boundary and the closed-field region is pushed out into the crust.

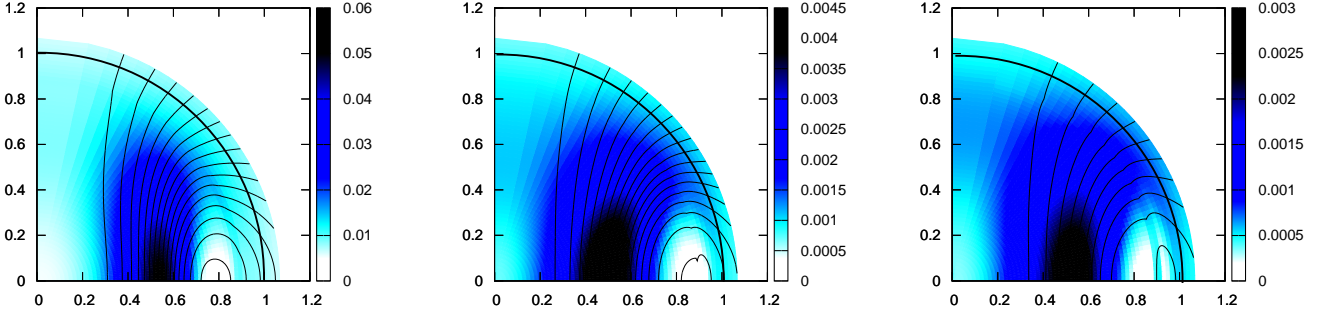


Figure 4. To check our results from figure 3 are not specific to the choice of flux function used there, we plot the corresponding sequence of equilibria for the case $M_N(u) = \kappa u^2$ here. The left, middle and right panels represent the cases $\langle B^{cc} \rangle > H_{c1}^{cc}$, $\langle B^{cc} \rangle \sim H_{c1}^{cc}$ and $\langle B^{cc} \rangle < H_{c1}^{cc}$, respectively. Although the core field distributions are different from figure 3, we again find that decreasing the field strength B tends to push the closed-field line region outwards into the crust.

the distortion of the star’s mass distribution, we now define the ellipticity of the star through the components of the quadrupole moment at the equator Q_{xx} and pole Q_{zz} :

$$\epsilon = \frac{Q_{xx} - Q_{zz}}{Q_{xx}}. \quad (41)$$

We expect the ellipticity to scale with the magnetic energy, i.e. $\epsilon \sim H_{c1}B$, as opposed to $\epsilon \sim B^2$ for normal matter (Jones 1975; Easson & Pethick 1977). In figure 7 we plot the ellipticity against field strength B for a variety of models, all with $M_N = \kappa u$ but different central critical fields, $H_{c1}(0) = 1, 2, 5 \times 10^{16}$ G. The field strengths are very high, as we need the distortion to be sufficiently large to resolve on our numerical grid. Most of our models are in the ‘high-field’ regime, with $B > H_{c1}$ at the crust-core boundary, but the data point for $H_{c1}(0) = 5 \times 10^{16}$ G represents a ‘medium-field’ model. We use this point to fix the gradient of line (c), and plot lines (a) and (b) at $\frac{1}{5}$ and $\frac{2}{5}$ of this gradient. These are seen to agree well with the data points for $H_{c1}(0) = 1 \times 10^{16}$ G and $H_{c1}(0) = 2 \times 10^{16}$ G, so we conclude that our results do indeed have the correct ellipticity scaling.

Using figure 7 and a similar plot for $M_N(u) = \kappa u^2$, we find the following ellipticity relations for a neutron star with

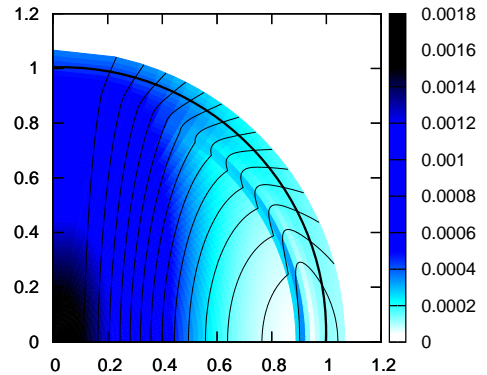


Figure 5. Poloidal field in a star with composition-gradient stratification in the core. This is a ‘low-field’ model, with $\langle B \rangle < H_{c1}$ at the crust-core boundary. The neutron and proton polytropic indices are $N_n = 0.6$ and $N_p = 1.5$.

a superconducting core:

$$\epsilon = 3.1 \times 10^{-8} \left(\frac{B_{\text{pole}}}{10^{12} \text{ G}} \right) \left(\frac{H_{c1}(0)}{10^{16} \text{ G}} \right) \quad (42)$$

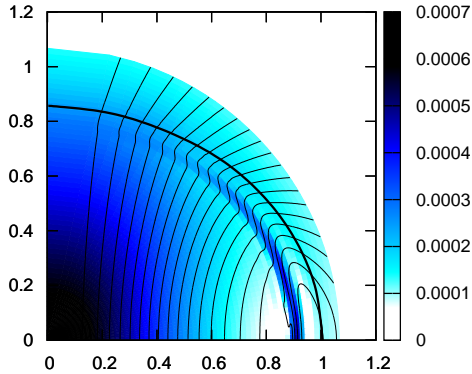


Figure 6. A rapidly-rotating unstratified star, again with a purely poloidal field and $\langle B \rangle < H_{c1}$ at the crust-core boundary. Rotation distorts the shape of the stellar surface and crust-core boundary, but otherwise the configuration is qualitatively similar to the other ‘low-field’ models shown in this section.

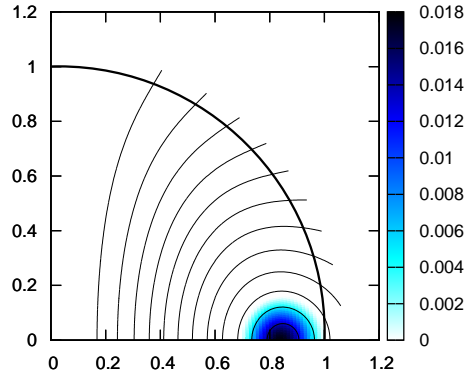


Figure 8. A mixed poloidal-toroidal magnetic field in a two-fluid core/single-fluid crust model, obeying normal MHD in both domains. We plot poloidal field lines, but this time the colour scale shows the magnitude of the toroidal field component only.

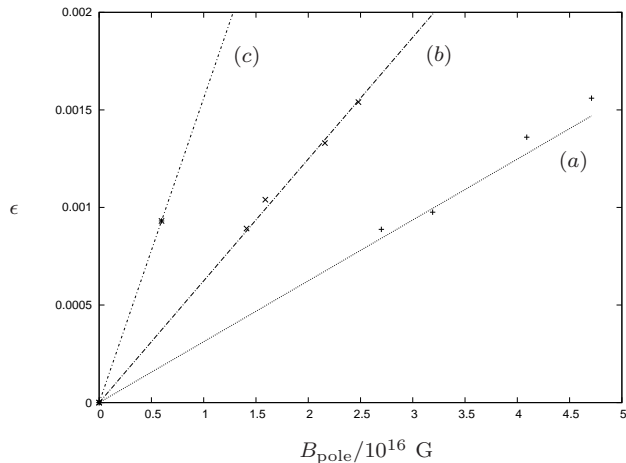


Figure 7. Scaling of magnetically-induced ellipticity ϵ with field strength at the polar cap B_{pole} . Lines (a), (b) and (c) are for models with a central critical field $H_{c1}(0) = 1, 2, 5 \times 10^{16}$ G respectively; these strong fields are needed to produce non-rotating stars with a sufficiently large distortion to be resolved on our numerical grid. Our results agree well with the expected scaling $\epsilon \sim H_{c1}B$.

for $M_N(u) = \kappa u$, and

$$\epsilon = 4.4 \times 10^{-8} \left(\frac{B_{\text{pole}}}{10^{12} \text{ G}} \right) \left(\frac{H_{c1}(0)}{10^{16} \text{ G}} \right) \quad (43)$$

for $M_N(u) = \kappa u^2$. Note that our new boundary condition has increased these values somewhat with respect to those reported in Lander (2013), where the prefactors were 2.5×10^{-8} for $M_N(u) = \kappa u$ and 3.4×10^{-8} for $M_N(u) = \kappa u^2$. An ellipticity often quoted for superconducting stars is the estimate for purely toroidal fields given by Cutler (2002), where the ellipticity prefactor for $(B/10^{12} \text{ G})$ is -1.6×10^{-9} (the negative sign reflects the prolate distortion which toroidal fields induce). We see that our poloidal-field results give distortions around 20 times bigger.

4.3 Mixed poloidal-toroidal fields

In the previous section we found that the ratio between the two fields B and H_{c1} at the crust-core boundary seemed to be the most important quantity dictating the structure of the poloidal field, giving us three classes of equilibria: ‘low-field’, ‘medium-field’ and ‘high-field’, depending on whether $\langle B^{cc} \rangle$ was smaller than, comparable to, or greater than H_{c1}^{cc} . We now turn to the general mixed-field case, where a toroidal component is present as well as the poloidal one. Since we found that neither stratification nor rotation have a significant effect on the field structure, we consider only unstratified and non-rotating models here.

As in the last section, we begin by presenting a typical field configuration in a NS with normal matter in the core and crust, for later comparison. Figure 8 shows a mixed poloidal-toroidal field, sometimes called a ‘twisted-torus field’ for its closed-field line geometry. The poloidal field is present throughout the interior and extends outside the star, whilst the toroidal component only exists in the small region of closed field lines, as dictated by equation (39). The maximum value of the toroidal component is comparable with that of the poloidal component, but it is globally weak, in the sense that it occupies a small volume; it only contributes 3% of the star’s magnetic energy.

In a superconducting star, the toroidal field must still be fitted inside closed field lines (equation (38)). Based on the very small closed-field line regions seen in the last section, we may therefore anticipate that any toroidal components will be confined to a tiny volume of the star. This is borne out by figure 9. The high-field model on the left-hand side is reminiscent of the normal-matter case shown in figure 8 — although whereas the toroidal field in the normal-matter star attains its maximum at the centre of the closed-field line region, in the superconducting star it vanishes there. In three dimensions, then, the toroidal component forms a hollow tube, as also seen in Lander (2013). This structure is in fact dictated by the form of the toroidal-field flux function; one can rearrange equation (24), using

$\Pi = B/\rho_p = \sqrt{B_{\text{pol}}^2 + B_\phi^2}/\rho_p$, to show that

$$B_\phi = \frac{B_{\text{pol}}f(u)}{\sqrt{\rho_p^2\varpi^2 - f^2(u)}} \quad (44)$$

— when B_{pol} vanishes, B_ϕ must too.

Moving to the middle panel of figure 9, for a ‘medium-field’ model, we see that the toroidal component has been pushed outwards, and in the right-hand panel — a ‘low-field’ star — the toroidal component exists only in the normal crust. In all three plots the toroidal field is locally comparable with the poloidal component, but globally extremely weak: from left to right, the percentages of magnetic energy in the toroidal component are 0.11, 0.0025 and 2.2×10^{-6} respectively.

5 DISCUSSION

The main conclusion of this work is that field configurations inside a superconducting neutron star may vary dramatically depending on the field strength, in contrast to normal-matter models where the field geometry is essentially independent of its strength. The reason is that, unlike normal matter, type-II superconductors have a characteristic field strength $H_{c1} \sim 10^{15}$ G, which is density-dependent and enters the governing equations of the system. Our results indicate that the crucial quantity dictating the equilibrium configuration is the ratio of B to H_{c1} at the crust-core boundary.

Within the context of our model, we report in table 1 the key features we would expect a neutron star’s interior field to have, based on its polar-cap field. This serves as a summary of the main results of this paper. For polar-cap fields below $\sim 5 \times 10^{13}$ G we expect discontinuities at the crust-core boundary and any toroidal component to be confined to the crust. The volume-averaged field for these ‘low-field’ models may be a factor of 7 stronger than than the observed polar-cap value. Our scheme has not converged to any models in the range $6 \times 10^{13} \text{ G} \lesssim B_{\text{pole}} \lesssim 2 \times 10^{14}$ G, presumably because of numerical limitations. Our ‘medium-field’ models start at around 2×10^{14} G and span an order of magnitude, covering typical magnetar values; for these configurations B_{pole} is typically about half of the average interior strength and the toroidal component begins to penetrate the core. In the ‘high-field’ range, up to $\sim 6 \times 10^{15}$ G, the toroidal component pervades more of the interior and the configuration begins to resemble the smooth solutions from stars with normal matter in the core and crust.

Superconductivity is destroyed for magnetic fields above the upper critical field H_{c2} , at which point one returns to the regime of normal MHD (Glampedakis, Andersson & Samuelsson 2011). This critical field is density-dependent, but for simplicity we will — rather arbitrarily — assume the destruction of superconductivity happens when the volume-averaged field $\bar{B} > 10^{16}$ G. Using our earlier code for a star with a normal-matter core (Lander, Andersson & Glampedakis 2012), we would expect this interior field to be attained for a polar-cap field of $B_{\text{pole}} \sim 5 \times 10^{15}$ G. Now using our superconducting models for an independent estimate of this field strength, we arrive at a reassuring similar value of $B_{\text{pole}} \sim 6 \times 10^{15}$ G.

Our naive estimates suggest that no known magnetar

has a field quite high enough to destroy superconductivity in the interior; the highest observed polar-cap field is 2×10^{15} G, for SGR 1806-20. Many of them *are*, however, in a range around $B_{\text{pole}} \sim 10^{14}$ G, corresponding roughly to the strength separating the qualitatively different ‘low’ and ‘medium’-field configurations in our work. As a magnetar’s field decays, our models indicate that it will need to rearrange substantially to adapt to its new equilibrium, with a surface field strength considerably lower than the interior average. This predicted rearrangement may play a role in the flaring and glitch activity observed for many magnetars.

In all our models the toroidal field component can be locally important (comparable in magnitude to the poloidal one), but is always globally insignificant. Accordingly, the toroidal component plays no role in the size of magnetically-induced distortions, and we expect it to be irrelevant for oscillations of our model neutron stars too. It may be relevant for a neutron star’s stability, however, as magnetic instabilities are typically local in nature. Recent work for normal-matter stars (Ciolfi & Rezzolla 2013) has found solutions with strong toroidal components by careful choices of the magnetic free functions entering the governing equations, but it seems less likely this would work in the context of a superconducting star, where the physics at the crust-core boundary has the strongest effect on the resultant equilibria.

The results in this paper suggest intriguing differences between the interior fields of neutron stars in the typical range for pulsars, $B \lesssim 5 \times 10^{13}$ G, and those in the magnetar range, $B \gtrsim 10^{14}$ G. At the same time, we should be cautious that our modelling of neutron star superconductivity here is quite primitive. Essentially, we have only managed to account for the basic features of a model (Baym, Pethick & Pines 1969) which is now more than forty years old! The most obvious pieces of physics missing from our models are entrainment — which results in an effective magnetic force on the neutrons in addition to the one on the protons — and interactions between neighbouring fluxtubes, expected for the range $H_{c1} < B < H_{c2}$ when fluxtubes become densely packed within the core.

In addition, neutron stars are likely to have an inner region where the superconductivity is of type I (Jones 2006; Glampedakis, Andersson & Samuelsson 2011), or could even be type-I throughout the core (Buckley, Metlitski & Zhitnitski 2004). At present there is no set of macroscopic smooth-averaged equations for this case, as would be needed to find equilibria in our approach. There may also be exotic physics at the transition between type-II and type-I superconductivity (Alford & Good 2008). Finally, if the density is high enough there could be an inner core of exotic matter, like hyperons or quarks (Alcock, Farhi & Olinto 1986). If we want a better understanding of magnetic-field physics in neutron stars, these difficult but interesting issues must be confronted.

ACKNOWLEDGEMENTS

I am pleased to thank Nils Andersson for his comments on the results presented here. This work is supported by the German Science Foundation (DFG) via SFB/TR7.

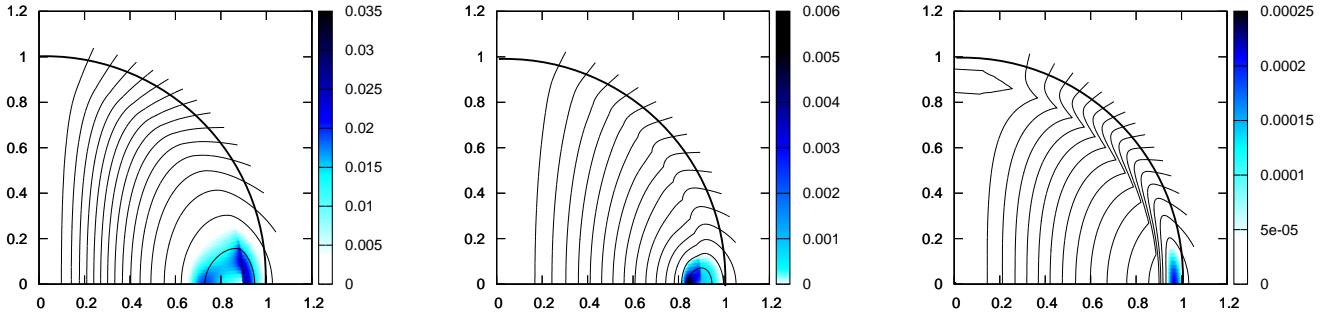


Figure 9. Mixed poloidal-toroidal field configurations in stars with a superconducting core and normal crust. We plot the poloidal field lines and use the colour scale to show the magnitude of the toroidal component only. As usual the plots, from left to right, show the ‘high’, ‘medium’ and ‘low’ field cases (determined by the ratio $\langle B^{cc} \rangle / H_{c1}^{cc}$). The fate of the toroidal-field component is tied to that of the closed field lines, through equations (38) and (39) — and so it too is seen to be expelled from the core and confined to the crust as the field strength B is decreased. In each case the toroidal component is locally strong but globally weak: its magnitude is comparable with that of the poloidal component in the same region, but its contribution to the magnetic energy is below 1%.

Table 1. Expected features of neutron star internal magnetic fields, for different polar-cap field strengths, based on our models. These results are for $M_N(u) = \kappa u$, but the case $M_N(u) = \kappa u^2$ is qualitatively similar.

polar-cap field	H_{c1}^{cc} vs B^{cc}	\bar{B}/B_{pole}	closed-field-line/toroidal-field region
$B_{\text{pole}} \lesssim 5 \times 10^{13}$ G	‘low’: $\langle B^{cc} \rangle \lesssim 0.4 H_{c1}^{cc}$	6 – 7	confined to crust
$2 \times 10^{14} \text{ G} \lesssim B_{\text{pole}} \lesssim 2 \times 10^{15}$ G	‘medium’: $0.4 H_{c1}^{cc} \lesssim \langle B^{cc} \rangle \lesssim H_{c1}^{cc}$	1.2 – 1.8	in crust and core, centred in crust
$2 \times 10^{15} \text{ G} \lesssim B_{\text{pole}} \lesssim 6 \times 10^{15}$ G	‘high’: $\langle B^{cc} \rangle \gtrsim H_{c1}^{cc}, \bar{B} < H_{c2}$	1.7	in crust and core, centred in core
$B_{\text{pole}} \gtrsim 5 \times 10^{15}$ G	normal matter: $\bar{B} > H_{c2}$	1.9	in crust and core, centred in core

REFERENCES

- Akgün T., Wasserman I., 2008, MNRAS 383, 1551
 Akgün T., Reisenegger A., Mastrano A., Marchant P., 2013 MNRAS, 433, 2445
 Akmal A., Pandharipande V. R., Ravenhall D. G., 1998, Phys. Rev. C 58, 1804
 Alcock C., Farhi E., Olinto A., 1986, ApJ 310, 261
 Alford M., Good G., 2008, Phys. Rev. B 78, 024510
 Anderson P.W., Itoh N., 1975, Nature 256, 25
 Antoniadis J. et al., 2013, Science 340, 448
 Bardeen J., Cooper L.N., Schrieffer J.R., 1957, Phys. Rev. 108, 1175
 Baym G., Pethick C., Pines D., 1969, Nature 224, 673
 Bonazzola S., Gourgoulhon E., 1996, A&A 312, 675
 Buckley K., Metlitski M. A., Zhitnitski A. R., 2004, Phys. Rev. Lett. 92, 151102
 Ciolfi R., Rezzolla L., 2013, arXiv:1306.2803
 Cutler C., 2002, Phys. Rev. D 66, 084025
 Demorest P. B., Pennucci T., Ransom S. M., Roberts M. S. E., Hessels J. W. T., 2010, Nature 467, 1081
 Easson I., Pethick C. J., 1977, Phys. Rev. D 16, 275
 Easson I., 1979, ApJ 228, 257
 Ginzburg V. L., Kirzhnits D.A., 1965, Soviet J. Exp. Th. Phys. 20, 1346
 Glampedakis K., Andersson N., Samuelsson L., 2011, MNRAS 410, 805
 Glampedakis K., Lander S.K., Andersson N., 2013, arXiv:1306.6881
 Gourgouliatos K. N., Cumming A., Reisenegger A., Armaza C., Lyutikov M., Valdivia J. A., 2013, arXiv:1305.6269
 Grad H., Rubin H., 1958, in Proc. 2nd Int. Conf. on Peaceful Uses of Atomic Energy, United Nations, Geneva, 31, 190
 Hachisu I., 1986, ApJ S. 61, 479
 Henriksson K., Wasserman I., 2013, MNRAS 431, 2986
 Ho W.C.G., Glampedakis K., Andersson N., 2012, MNRAS 422, 2632
 Jones P.B., 1975, Astrophys. Space Sci. 33, 215
 Jones P.B., 1987, MNRAS 228, 513
 Jones P.B., 2006, MNRAS 371, 1327
 Kaspi V., 2010, P.N.A.S. 107, 7147
 Lander S.K., Jones D.I., 2009, MNRAS 395, 2162
 Lander S.K., Andersson N., Glampedakis K., 2012, MNRAS 419, 732
 Lander S.K., 2013, Phys. Rev. Lett. 110, 071101
 Mastrano A., Melatos A., Reisenegger A., Akgün T., 2011, MNRAS 417, 2288
 Mendell G., 1991, ApJ 380, 515
 Mestel L., Takhar H.S., 1972, MNRAS 156, 419
 Migdal A.B., 1959, Nuclear Phys. 13, 655
 Page D., Prakash M., Lattimer J.M., Steiner A.W., 2011, Phys. Rev. Lett. 106, 081101
 Pons J.A., Miralles J.A., Geppert U., 2009, A&A 496, 207
 Prix R., Comer G. L., Andersson N., 2002, A&A 381, 178
 Reisenegger A., 2009, A&A 499, 557
 Roberts P.H., 1981, Quart. J. Mech, Appl. Math. 34, 327
 Sauls J. A., 1989, in Timing neutron stars, ed. H. Ögelman, E. P. J. van den Heuvel, Kluwer Academic, New York
 Sedrakian A., 2005, Phys. Rev. D. 71, 083003
 Shafranov V.D., 1958, Soviet J. Exp. Th. Phys. 6, 545
 Shternin P.S., Yakovlev D.G., Heinke C.O., Ho W.C.G., Patnaude D.J., 2011, MNRAS 412, L108
 Spruit H. C., 2009, in Proc. I.A.U. Symposium, ed. Strassmeier K.G., Kosovichev A.G. and Beckman, J.E., 259, 61
 Tayler R.J., 1973, MNRAS 161, 365
 Thompson C., Duncan R.C., 1996, ApJ 473, 322
 Tilley D.R., Tilley J., 1990, Superfluidity and Superconductivity, IOP Publishing, London

- Tinkham M., 1996, Introduction to Superconductivity, McGraw-Hill, Singapore
 Tomimura Y., Eriguchi Y., 2005, MNRAS 359, 1117
 Viganò D., Rea N., Pons J.A., Perna R., Aguilera D.N., Miralles J.A., 2013, arXiv:1306.2156
 Yoshida S., Kiuchi K., Shibata M., 2012, Phys. Rev. D 86, 044012
 Wright G.A.E., 1973, MNRAS 162, 339

APPENDIX A: DERIVATION OF THE ‘GRAD-SHAFRANOV’ EQUATION FOR A SUPERCONDUCTOR

In section 3.2 we established the basic results of axisymmetric MHD, which are independent of the form of the magnetic force. We now specialise to the fluxtube tension force discussed in section 2:

$$\mathfrak{F}_{\text{mag}} = -\frac{1}{4\pi} \left[\mathbf{B} \times (\nabla \times \mathbf{H}_{c1}) + \rho_p \nabla \left(B \frac{\partial H_{c1}}{\partial \rho_p} \right) \right], \quad (\text{A1})$$

where $\mathbf{H}_{c1} = H_{c1} \hat{\mathbf{B}}$ is the critical field, pointing in the same direction as \mathbf{B} . To our order of working $H_{c1} = h_c \rho_p / \varepsilon_*$, where h_c and ε_* are constants (Glampedakis, Andersson & Samuelsson 2011). We will assume zero entrainment (meaning $\varepsilon_* = 1$), otherwise there will be a magnetic force acting on the neutrons too. Equation (A1) now becomes

$$-\frac{4\pi}{h_c} \mathfrak{F}_{\text{mag}} = \rho_p \nabla B + \mathbf{B} \times \left(\rho_p \nabla \times \hat{\mathbf{B}} + \nabla \rho_p \times \hat{\mathbf{B}} \right). \quad (\text{A2})$$

At this point it is convenient to define a ‘unit current’ $\hat{\mathbf{j}} \equiv \nabla \times \hat{\mathbf{B}}$; as in the single-fluid case (Lander & Jones 2009) it may be shown that

$$\hat{\mathbf{j}} = \frac{1}{\varpi} \nabla(\varpi \hat{B}_\phi) \times \mathbf{e}_\phi + \hat{j}_\phi \mathbf{e}_\phi. \quad (\text{A3})$$

Decomposing the bracketed terms from the right-hand side of equation (A2) into poloidal and toroidal components gives, after some rearrangement,

$$\begin{aligned} \rho_p \nabla \times \hat{\mathbf{B}} + \nabla \rho_p \times \hat{\mathbf{B}} &= \frac{1}{\varpi} \nabla(\rho_p \varpi \hat{B}_\phi) \times \mathbf{e}_\phi \\ &+ \left(\rho_p \hat{j}_\phi - \frac{\nabla \rho_p \cdot \nabla u}{\varpi B} \right) \mathbf{e}_\phi \end{aligned} \quad (\text{A4})$$

so the magnetic force becomes

$$\begin{aligned} -\frac{4\pi}{h_c} \mathfrak{F}_{\text{mag}} &= \rho_p \nabla B + \frac{1}{\varpi} \mathbf{B} \times \left(\nabla(\rho_p \varpi \hat{B}_\phi) \times \mathbf{e}_\phi \right) \\ &+ \left(\rho_p \hat{j}_\phi - \frac{\nabla \rho_p \cdot \nabla u}{\varpi B} \right) \mathbf{B} \times \mathbf{e}_\phi. \end{aligned} \quad (\text{A5})$$

Noting that

$$\mathbf{B} \times \mathbf{e}_\phi = \mathbf{B}_{\text{pol}} \times \mathbf{e}_\phi = -\frac{\nabla u}{\varpi}, \quad (\text{A6})$$

and using standard vector identities, we may rearrange (A5) into the form:

$$\begin{aligned} -\frac{4\pi}{h_c} \mathfrak{F}_{\text{mag}} &= \rho_p \nabla B + \frac{1}{\varpi^2} \nabla u \times \nabla(\rho_p \varpi \hat{B}_\phi) + \frac{B_\phi}{\varpi} \nabla(\rho_p \varpi \hat{B}_\phi) \\ &+ \left(\frac{\nabla \rho_p \cdot \nabla u}{\varpi B} - \rho_p \hat{j}_\phi \right) \frac{\nabla u}{\varpi}. \end{aligned} \quad (\text{A7})$$

In axisymmetry, $\mathfrak{F}_{\text{mag}}$ has no toroidal component. Examining the above expression, we see all terms are poloidal except the following one, which must therefore be zero:

$$\frac{1}{\varpi^2} \nabla u \times \nabla(\rho_p \varpi \hat{B}_\phi) = 0. \quad (\text{A8})$$

Hence we can remove this term from the magnetic force to arrive at our ‘interim’ result for $\mathfrak{F}_{\text{mag}}$:

$$\begin{aligned} -\frac{4\pi}{h_c} \mathfrak{F}_{\text{mag}} &= \rho_p \nabla B + \frac{B_\phi}{\varpi} \nabla(\rho_p \varpi \hat{B}_\phi) \\ &+ \left(\frac{\nabla \rho_p \cdot \nabla u}{\varpi B} - \rho_p \hat{j}_\phi \right) \frac{\nabla u}{\varpi}. \end{aligned} \quad (\text{A9})$$

We now have the same dichotomy as for the normal-MHD case: satisfying (A8) leads to a mixed-field case, or a purely-toroidal case. For the former, we require that ∇u and $\nabla(\rho_p \varpi \hat{B}_\phi)$ be parallel, which leads to

$$\rho_p \varpi \hat{B}_\phi = f(u) \quad (\text{A10})$$

for some function f . In the special case $f(u) = 0$ the field is purely poloidal. Alternatively, we can satisfy (A8) by taking $\nabla u = 0$, so that our field is purely toroidal. We begin with this latter, simpler case.

A1 Toroidal fields

The purely-toroidal field case is no more involved than the corresponding derivation for normal matter. It has been studied in earlier papers (Akgün & Wasserman 2008; Lander, Andersson & Glampedakis 2012), but we include the results for completeness. From (A9), we have $\nabla u = 0$ and so the expression for the magnetic force reduces to

$$\mathfrak{F}_{\text{mag}} = -\frac{h_c}{4\pi} \frac{1}{\varpi} \nabla(\varpi \rho_p B_\phi). \quad (\text{A11})$$

Now since $\nabla \times (\mathfrak{F}_{\text{mag}} / \rho_p) = 0$ we have

$$0 = \nabla(\varpi \rho_p) \times \nabla(\varpi \rho_p B_\phi) \quad (\text{A12})$$

and hence the arguments of the two gradient operators must be related by some function η :

$$\eta(\varpi \rho_p) = \varpi \rho_p B_\phi. \quad (\text{A13})$$

Putting this into (A11), using $\mathfrak{F}_{\text{mag}} = \rho_p \nabla M$ and defining $\zeta \equiv \varpi \rho_p$ we get

$$\nabla M = -\frac{h_c}{4\pi} \frac{1}{\zeta} \nabla \eta(\zeta) = -\frac{h_c}{4\pi} \frac{1}{\zeta} \frac{d\eta}{d\zeta} \nabla \zeta \quad (\text{A14})$$

where the corresponding magnetic field is

$$\mathbf{B} = B_\phi \mathbf{e}_\phi = \frac{\eta(\zeta)}{\zeta} \mathbf{e}_\phi. \quad (\text{A15})$$

Equation (A14) gives the magnetic force in a form that allows for direct integration of the proton Euler equation and no additional equation for the magnetic field is needed.

A2 Mixed poloidal-toroidal fields

We return to the general equation for the magnetic force (A9). The B_ϕ terms in this expression may be replaced using the relation (A10) and the left-hand side may be rewritten

using $\mathfrak{F}_{\text{mag}} = \rho_p \nabla M$. Now applying the chain rule to the resulting $\nabla f(u)$ term and rearranging, we have

$$-\frac{4\pi}{h_c} \nabla M - \nabla B = \left(\frac{Bf}{\rho_p^2 \varpi} \frac{df}{du} + \frac{\nabla \rho_p \cdot \nabla u}{\rho_p \varpi B} - \hat{j}_\phi \right) \frac{\nabla u}{\varpi}. \quad (\text{A16})$$

At this point in the normal-matter derivation one dots \mathbf{B} into this equation, showing that $\mathbf{B} \cdot \nabla M = 0$; together with $\mathbf{B} \cdot \nabla u = 0$, this gives the important result $M = M(u)$. For superconducting matter this is no longer true. Instead, let us define a new function

$$y = \frac{4\pi M}{h_c} + B. \quad (\text{A17})$$

Now, dotting \mathbf{B} into equation (A16) we have

$$-\mathbf{B} \cdot \nabla y = \frac{1}{\varpi} \left(\frac{Bf}{\rho_p^2 \varpi} \frac{df}{du} + \frac{\nabla \rho_p \cdot \nabla u}{\rho_p \varpi B} - \hat{j}_\phi \right) \mathbf{B} \cdot \nabla u = 0 \quad (\text{A18})$$

— we know that $\mathbf{B} \cdot \nabla u = 0$, and so $\mathbf{B} \cdot \nabla y = 0$ too. But this in turn means that ∇u and ∇y are parallel, so:

$$y = y(u) \quad (\text{A19})$$

and hence

$$-\frac{dy}{du} \nabla u = \left(\frac{Bf}{\rho_p^2 \varpi} \frac{df}{du} + \frac{\nabla \rho_p \cdot \nabla u}{\rho_p \varpi B} - \hat{j}_\phi \right) \frac{\nabla u}{\varpi}. \quad (\text{A20})$$

For $\nabla u \neq 0$ we then get a relation between the functions y and f :

$$y'(u) = -\frac{B}{\varpi^2 \rho_p^2} f(u) f'(u) - \frac{\nabla \rho_p \cdot \nabla u}{\varpi^2 \rho_p B} + \frac{\hat{j}_\phi}{\varpi}. \quad (\text{A21})$$

Let us now get rid of \hat{j}_ϕ in favour of an expression in terms of u :

$$\hat{j}_\phi = [\nabla \times \hat{\mathbf{B}}]_\phi = -\frac{1}{\varpi B} \left(\Delta_* u - \frac{\nabla B \cdot \nabla u}{B} \right), \quad (\text{A22})$$

using the same Δ_* operator as for the Grad-Shafranov equation (13). As for normal MHD, this step gives \hat{j}_ϕ in terms of a differential operator acting on u (albeit a more complicated one). Now using this to replace \hat{j}_ϕ in equation (A21), we have

$$\Delta_* u - \frac{\nabla B \cdot \nabla u}{B} + \frac{\nabla \rho_p \cdot \nabla u}{\rho_p} = -\frac{B^2}{\rho_p^2} f f' - \varpi^2 B y'. \quad (\text{A23})$$

Since the quantity B/ρ_p appears frequently in the above expression, let us call this Π . One final rearrangement of the magnetic force expression then gives our final result, a ‘Grad-Shafranov’ equation for type-II superconductors:

$$\Delta_* u - \frac{\nabla \Pi \cdot \nabla u}{\Pi} = -\varpi^2 \rho_p \Pi y' - \Pi^2 f f'. \quad (\text{A24})$$

One could now replace the Π terms by quantities involving u , since

$$\Pi \equiv \frac{B}{\rho_p} = \frac{|\nabla u|}{\sqrt{\varpi^2 \rho_p^2 - f^2}}, \quad (\text{A25})$$

but the result is forbidding and not obviously useful.

APPENDIX B: NUMERICAL METHOD

B1 The differential operator in equation (A24)

As written in equation (A24), our problem features a very unfamiliar differential operator ($\Delta_* - \frac{1}{\Pi} \nabla \Pi \cdot \nabla$) acting on the

streamfunction, and we would have to find a Green’s function to invert it. Even the normal-matter Grad-Shafranov equation (13), however, is unconventional in having u dependence on the left and right-hand sides. It seems equally legitimate to move the $\nabla \Pi \cdot \nabla u / \Pi$ term to the right-hand side, especially since we will use an iterative scheme which should gradually update both sides of the equation and approach a consistent solution. Whether or not this approach is acceptable can be decided based on if the scheme converges, and if the resultant configuration satisfies the equilibrium form of the virial theorem, discussed later in this section.

Accordingly, we now proceed in a similar manner to that previously used to solve the Grad-Shafranov equation (Tomimura & Eriguchi 2005; Lander & Jones 2009), converting the magnetic equation (A24) into a Poisson-like equation, which may then be solved using familiar Green’s-function methods. For this we use the following relation between the Δ_* and Laplacian operators:

$$\Delta_* u = \frac{\varpi}{\sin \phi} \nabla^2 \left(\frac{u \sin \phi}{\varpi} \right). \quad (\text{B1})$$

Equation (A24) then takes the form:

$$\nabla^2 \left(\frac{u \sin \phi}{\varpi} \right) = - \left[-\frac{\nabla \Pi \cdot \nabla u}{\varpi \Pi} + \varpi \rho_p \Pi y'(u) + \frac{\Pi^2}{\varpi} f(u) f'(u) \right] \sin \phi. \quad (\text{B2})$$

In integral form this is:

$$u = \frac{\varpi}{4\pi \sin \phi} \int \left[-\frac{\nabla \tilde{\Pi} \cdot \nabla \tilde{u}}{\tilde{\varpi} \tilde{\Pi}} + \tilde{\varpi} \tilde{\rho}_p \tilde{\Pi} y'(\tilde{u}) + \frac{\tilde{\Pi}^2}{\tilde{\varpi}} f(\tilde{u}) f'(\tilde{u}) \right] \frac{\sin \tilde{\phi}}{|\mathbf{r} - \tilde{\mathbf{r}}|} d\tilde{\mathbf{r}}, \quad (\text{B3})$$

denoting dummy variables with tildes.

B2 Iterative scheme

As in Lander, Andersson & Glampedakis (2012), our numerical method is based on the Hachisu self-consistent field method (Hachisu 1986), an iterative scheme originally used for rotating unmagnetised stars. The method finds solutions to the equilibrium equations in integral form, by progressively updating the density distribution to satisfy some user-specified surface distortion. For stars with magnetic fields and normal matter, it is quite easily generalised by including the integral form of the Grad-Shafranov equation in the scheme (Tomimura & Eriguchi 2005; Lander, Andersson & Glampedakis 2012), and is robust. The extra nonlinearities of the new magnetic equation (B3) cause the method difficulties, however — with direct implementation resulting in a non-convergent, unstable scheme. We have found these can be cured by ‘normalising’ the magnetic integral by the maximum value attained by Π (dividing by Π_{max} when solving the integral and multiplying again afterwards) and by using underrelaxation.

The underrelaxation step works by updating the streamfunction only partially at each iterative step. If u_{new}^* is the result of integrating (B3), then *fully* updating the streamfunction would entail discarding the form u_{old} from

the last iterative step and setting $u_{\text{new}} = u_{\text{new}}^*$ for the new streamfunction; instead we update by using

$$u_{\text{new}} = (1 - \omega)u_{\text{old}} + \omega u_{\text{new}}^*. \quad (\text{B4})$$

Clearly $\omega = 1$ gives us the conventional full-update case. When solving (B3), we have found that the most successful value of the underrelaxation parameter ω varies with the grid resolution and the input parameters, but is typically in the range 0.01 – 0.2.

The complete iterative scheme, which converges successfully, takes the form:

0. For the initial conditions, start with simple trial guesses for ρ_n, ρ_p and u ;

1. Calculate the gravitational potential Φ from the ρ_n and ρ_p distributions and Poisson's equation (5);

2. Calculate Π from u using (A25);

3. Calculate the new magnetic streamfunction u from its value at the previous iteration u_{old} , using the magnetic Poisson equation (B3) with u_{old} , Π and ρ_p in the integrand. Divide the integrand by Π_{max} before evaluation, multiply again afterwards and employ the underrelaxation step (B4);

4. Evaluate the proton-fluid Euler at the equatorial and polar surfaces, using boundary conditions on $\tilde{\mu}_p$; this gives two equations which fix Ω^2 and then the integration constant for the proton Euler equation;

5. We are now able to use the proton Euler to find $\tilde{\mu}_p$ throughout the star;

6. Evaluate the difference-Euler at the equatorial neutron-fluid surface to find the integration constant for the difference-Euler;

7. Now use the difference-Euler to find $\tilde{\mu}_n$ throughout the star;

8. Calculate the new density distributions from the chemical potentials, as in Lander, Andersson & Glampedakis (2012);

9. Return to step 1 using the new ρ_n, ρ_p and u ; repeat procedure until satisfactory convergence is achieved, i.e. until the fractional changes in quantities at consecutive iterative steps is less than some small tolerance (usually 10^{-4}).

The input parameters for any equilibrium configuration are the surface distortion $r_{\text{pole}}/r_{\text{eq}}$, the proton and neutron polytropic indices N_p, N_n and the constants κ and a , related to the strengths of the poloidal and toroidal field components. The iterative process described here typically takes 100–1000 steps. By comparison, the code for normal matter using in Lander, Andersson & Glampedakis (2012) usually converged within ten. We ensure the crust-core boundary is well resolved by having a larger number of radial grid points than angular ones, usually 480×180 .

B3 Tests of the numerical scheme

To check that our resulting solutions are truly equilibria, we want to use the virial theorem, as in the normal-MHD case. The virial theorem states that a certain combination of energies gives the acceleration of the system (the second time-derivative of the moment of inertia I):

$$2T + \mathcal{E}_{\text{mag}} + W + 3(\gamma_n - 1)U_n + 3(\gamma_p - 1)U_p = \frac{1}{2} \frac{d^2 I}{dt^2}, \quad (\text{B5})$$

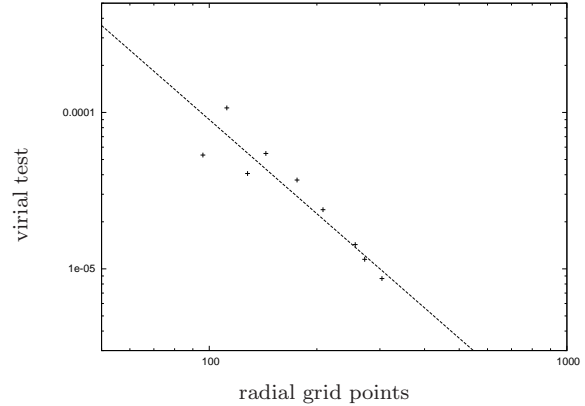


Figure B1. The virial test measures the deviation of our results from the expected value of zero for an equilibrium, and therefore quantifies our numerical error. We plot this for the same poloidal-field equilibrium at different grid resolutions. The line shows the expected scaling for second-order convergence; our results agree well with this.

for our double-polytrope EOS. For an equilibrium we want $\ddot{I} = 0$, up to the accuracy of our numerical scheme.

Our results should approach the continuum solution, where $\ddot{I} = 0$, at infinite resolution. We can check this by using the following quantity as a diagnostic:

$$\text{virial test} \equiv \frac{2T + \mathcal{E}_{\text{mag}} + W + 3(\gamma_n - 1)U_n + 3(\gamma_p - 1)U_p}{|W|}. \quad (\text{B6})$$

This is plotted in figure B1, for different radial grid resolutions. The plot shows that the results converge at second order, the intended order of the code. In the main part of the paper we also perform a more physical sanity check: checking that the magnetically-induced distortion to the star has the correct scaling of $\epsilon \sim H_{c1} B$. Figure 7 shows that our results agree convincingly with this relation.